Pharmaceutical Research, Vol. 24, No. 11, November 2007 (© 2007)
DOI: 10.1007/s11095-007-9402-5

Research Paper

Peritoneal Macrophage Uptake, Pharmacokinetics and Biodistribution of Macrophage-Targeted PEG-fMLF (*N*-Formyl-Methionyl-Leucyl-Phenylalanine) Nanocarriers for Improving HIV Drug Delivery

Li Wan,[1] Shahriar Pooyan,[1] Peidi Hu,[1] Michael J. Leibowitz,[2,3] Stanley Stein,[1] and Patrick J. Sinko[1,3,4,5]

Received May 9, 2007; accepted June 28, 2007; published online August 15, 2007

Purpose. To assess *in vivo* macrophage targeting potential of PEG-fMLF nanocarriers and to investigate their biodistribution, peritoneal macrophage uptake, and pharmacokinetics.
Methods. Multiple copies of fMLF were conjugated to purchased and novel (branched, peptide-based) PEG nanocarriers. Peritoneal macrophage uptake was evaluated in mice 4 hours after IP administration of fluorescence-labeled PEG-fMLF nanocarriers. Pharmacokinetics and biodistribution were determined in rats after IV administration of tritiated PEG-fMLF nanocarriers.
Results. Attachment of one, two, or four fMLF copies increased uptake in macrophages by 3.8-, 11.3-, and 23.6-fold compared to PEG without fMLF. Pharmacokinetic properties and tissue distribution also differed between nanocarriers with and without fMLF. Attachment of fMLF residues increased the $t_{1/2}$ of PEG_{5K} by threefold but decreased the $t_{1/2}$ of PEG_{20K} by 40%. Attachment of fMLF increased accumulation of nanocarriers into macrophages of liver, kidneys and spleen. However, on a molar basis, penetration was equivalent suggesting nanocarrier size and targeting moieties are important determinants.
Conclusions. These results demonstrate the feasibility for targeting macrophages, a primary HIV reservoir site. However, these studies also suggest that balancing peripheral tissue penetration (a size-dependent phenomenon) *versus* target cell uptake specificity remains a challenge to overcome.

KEY WORDS: biodistribution; HIV; PEG-fMLF nanocarrier; peritoneal macrophage; pharmacokinetic.

INTRODUCTION

Human immunodeficiency virus type 1 (HIV-1) infection is recognized as the major cause of impaired immune system function that leads to disease progression and death in patients with acquired immunodeficiency syndrome (AIDS). Numerous advances in antiretroviral drug therapy have been made with the advent of highly active antiretroviral therapy (HAART) (1), a multiple drug treatment regimen. Despite these advances, curing HIV infection has remained an elusive goal due to many challenges including low and fluctuating drug concentrations due to poor drug absorption or patient non-adherence (2), the presence of viral reservoirs and sanctuary sites (3), and drug toxicity during chronic high dose therapy (4). Highly potent drugs already exist but inefficient *in vivo* delivery limits their usefulness resulting in clinical "potency" viewed as "on the threshold with little margin for error" (4). Among the major causes of HIV treatment failure, insufficient drug exposure due to poor adherence to treatment regimens, inadequate and variable drug absorption and pharmacokinetics, or an inability of the agents to penetrate viral reservoirs are where little progress has been made and efforts are generally lacking. This, combined with poor adherence to clinical regimens and the inability to eradicate HIV from tissue and cell compartments, strongly suggests an urgent need for targeted drug delivery approaches. The explosive growth of nanotechnology in the past decade offers great yet unfulfilled promise in the field of drug delivery. It is hypothesized that by using targeted nanoparticle drug delivery systems, anti-HIV drugs can accumulate in HIV-infected tissues or cells selectively and quantitatively, while their concentration in non-infected tissues or cells should be much lower (5–7). Therefore, side effects are reduced, lower doses are needed and drug administration regimens are simplified (6). An ideal anti-HIV nanoscale drug delivery system needs to specifically target HIV infected sites, must have prolonged body persistence (i.e., a balance between circulation in plasma and target tissue penetration), and needs to be flexible enough in design to incorporate different combinations of targeting moieties and anti-HIV drugs.

[1] Department of Pharmaceutics, Ernest Mario School of Pharmacy, Rutgers, The State University of New Jersey, 160 Frelinghuysen Road, Piscataway, New Jersey 08854, USA.
[2] Department of Molecular Genetics, Microbiology & Immunology, University of Medicine and Dentistry of New Jersey-Robert Wood Johnson Medical School, Piscataway, New Jersey, USA.
[3] Cancer Institute of New Jersey, New Brunswick, New Jersey 08903, USA.
[4] Environmental and Occupational Health Science Institute, Piscataway, New Jersey, USA.
[5] To whom correspondence should be addressed. (e-mail: sinko@rci.rutgers.edu)

Cells of the macrophage lineage play an important role in the initial stage of HIV-1 infection and continue to do so throughout the course of infection (8). Productively infected macrophages have been found in both untreated patients and those receiving HAART (9). HIV-1 infection of macrophages can be productive but noncytopathic, permitting macrophages to serve as long-lived sources of HIV production (9). More importantly, they represent major viral reservoirs and are responsible for the relapse of the infection and resistance development on discontinuation of treatment. The tissue distribution of macrophages defines the anatomical reservoirs of HIV. In the body, macrophages colonize the primary lymphoid organs such as fetal bone marrow, liver, thymus and secondary lymph organs such as spleen, adult bone marrow, lymph nodes, gut- and mucosal-associated lymphoid tissue (GALT and MALT), in addition to other major organs such as the brain, lungs, kidney (10). Throughout the course of HIV infection, macrophages have been implicated in carrying virus across the blood–brain barrier and establishing and maintaining HIV infection within the central nervous system (CNS), probably the most important anatomical HIV reservoir. *In situ* hybridization and immunohistochemical analyses revealed that tissue macrophages in the lymph nodes, spleen, gastrointestinal tract, liver, and kidney sustain high plasma virus loads in rhesus macaques after the depletion of $CD4^+$ T cells by a highly pathogenic simian immunodeficiency virus/HIV type 1 chimera (SHIV) (11). Viral particles have also been identified in kidney (12), brain (13) and the cerebrospinal fluid (14). There are many more HIV-1 infected cells in lymph nodes than in the blood, which in any case contains fewer than 2% of total body lymphocytes (15). Taken together, it is clear that macrophages are not only a primary target of HIV infection in patients but they are an important source, in addition to $CD4^+$ T-lymphocytes, of HIV persistence during HAART (16,17). Therefore, drug delivery to macrophages represents a key challenge for eradicating HIV and improving anti-HIV therapy.

For these reasons, therapeutic strategies aimed at delivering anti-HIV drugs specifically to macrophages to achieve sufficient concentrations and control of HIV replication have been explored by our group (18). Macrophages possess various receptors such as formyl peptide receptors, mannose receptors, Fc receptors, complement and many other receptors (19–21). These surface receptors determine the control of activities such as activation, recognition, endocytosis, secretion etc. and potentially offer a targeting enhancing option via receptor-mediated endocytosis. A number of natural ligands for macrophage targeting have been explored. A previous report by Pooyan *et al.* (18) illustrated the potential of PEG nanocarrier bearing multiple copies of fMLF for improving *in vitro* macrophage targeting. Recently we showed that the conjugation of multiple targeting fMLF peptides to a PEG polymer resulted in enhanced uptake into macrophages *in vitro* while the number of attached copies of fMLF determined extent of uptake (Bioconj Chem 2007, submitted). Therefore, it is imperative that the relationship between the *in vivo* tissue dispositional properties and/or cellular uptake and structural characteristics of nanocarriers be further studied. In the present study, peritoneal macrophage uptake, pharmacokinetic and biodistribution of PEG-fMLF nanocarriers were investigated to assess their potential of *in vivo* macrophage targeting. The results demonstrate the feasibility of using macrophage-targeted nanocarriers for enhancing drug uptake in macrophages residing in tissues but re-emphasize the need to carefully design nanoscale delivery systems to achieve a good balance of body persistence and tissue penetration properties.

MATERIALS AND METHODS

Materials

N-formyl-met-leu-phe-lys-cys-amide and the backbone peptides acetyl-Cys(thiopyridine)–(β-Ala-β-Ala-Lys)$_4$-amide were synthesized via Fmoc chemistry by the W.M. Keck Facility (New Haven, CT). NHS-PEG-VS (vinyl sulfone) (MW ~5 kDa), mPEG-maleimide (MAL) (MW ~5.5 kDa), mPEG-(maleimide)$_2$ (MW ~5.5 kDa) and mPEG-NH_2 (MW ~5 kDa) were obtained from Nektar Therapeutics (Huntsville, AL). *N*-succinnimidyl-[2, 3-^{3}H]-propionate was purchased from Amersham Bioscience (Piscataway, NJ). Propionic anhydride, dimethylformamide(DMF), diisopropylethylamine(DIEA), acetonitrile (ACN), trifluoroacetic acid (TFA), ether and other chemical reagents were purchased from Sigma-Aldrich (St. Louis, MO). Frozen young rabbit plasma was purchased from PEL-Freez Biologicals (Rogers, AR). Solvable™ was purchased from PerkinElmer Life and Analytical Sciences, Inc. (Waltham, MA) for the solubilization of wet tissues and blood.

Synthesis of Fluorescein-Labeled PEG-fMLF Nanocarriers

Two millimoles mPEG$_{5K}$-maleimide or mPEG$_{5K}$-(maleimide)$_2$ was dissolved in 1 ml phosphate-buffered saline (PBS, pH=7.4) at room temperature. To this were added three equivalents of fMLFKC (Scheme 1). The reaction was stirred overnight at room temperature. The excess solvent was removed under reduced pressure. The solid PEGylated product was further reacted with three equivalents of NHS-carboxyfluorescein and 1% DIEA in 500 μl DMF. For control, 1 mmol mPEG$_{5k}$-NH_2 were reacted with three equivalents of NHS-carboxyfluorescein and 1% DIEA in 500 μl DMF to yield mPEG$_{5k}$-fluorescein. The reaction was stirred for 3 h at room temperature. The final product was recrystallized from cold ether, washed three times to remove impurities and dried under vacuum. The dried product was then dissolved in ~5 ml ddH_2O and was dialyzed against ddH_2O for 2 days in the dark. The solution was dried under vacuum to yield the purified product.

To achieve a branched shape and multiple coupling sites, peptide-backbone PEG nanocarriers were designed and synthesized (Scheme 1C). For 4 copies fMLF PEG nanocarriers (Scheme 1C), 2 mmol of the backbone peptide acetyl-Cys(thiopyridine)-[β-Ala-β-Ala-Lys]$_4$-amide was reacted with two equivalents of NHS-PEG$_{5k}$-VS and 1% DIEA in 500 μl DMF. The reaction was carried out at room temperature for 3 h. The product acetyl-Cys(thiopyridine)-[β-Ala-β-Ala-Lys(PEG$_{5k}$-VS)]$_4$-amide was purified by size exclusion chromatography with TSK Gel-3000PW column. The pooled fractions containing the product were dried under vacuum. Then this PEGylated intermediate was dissolved in 1 ml phosphate-buffered saline (PBS, pH=7.4) at room temperature. To this were added three equivalents of

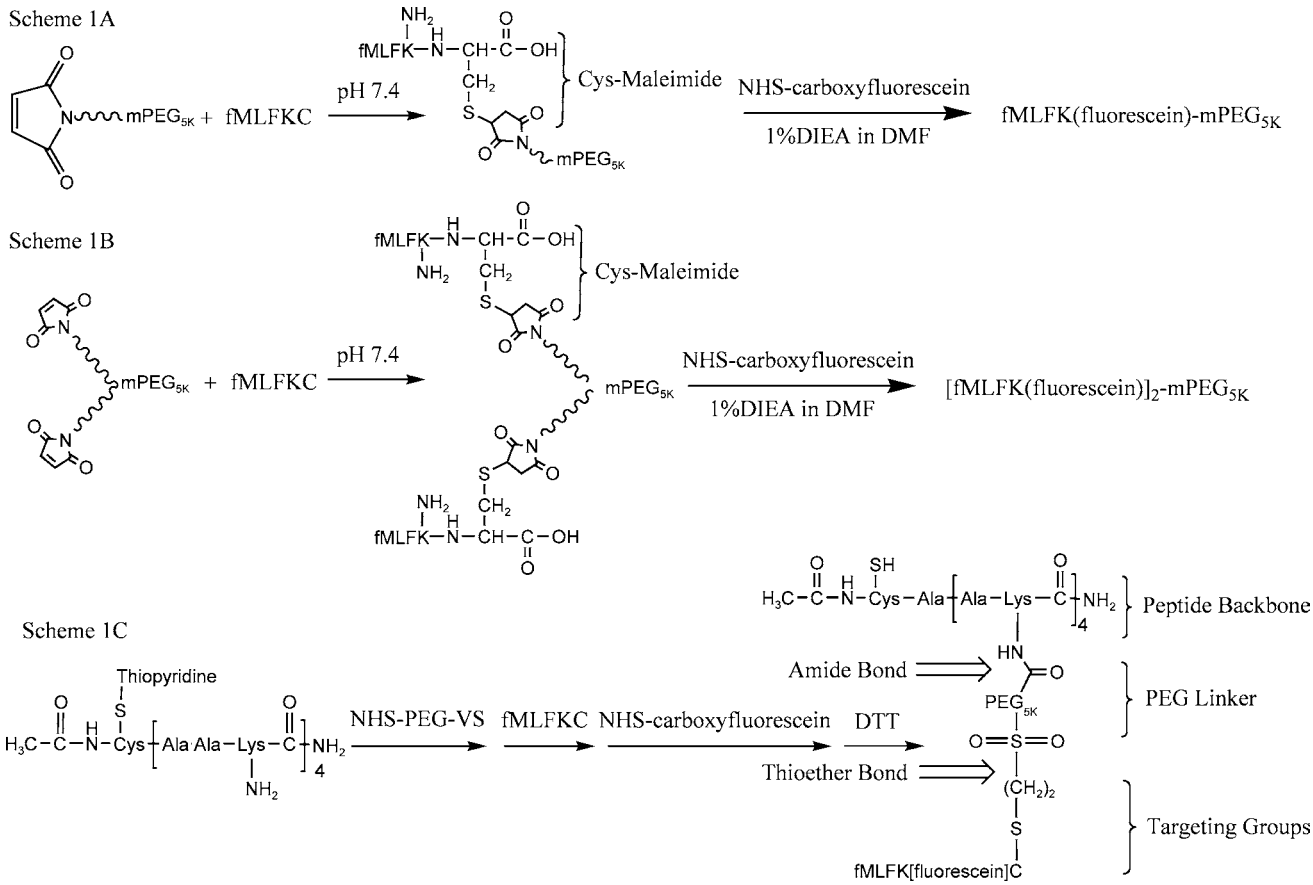

Scheme 1. Synthesis schemes of fluorescein-labeled PEG-fMLF nanocarriers with 1 (A), 2 (B) and 4 (C) copies of fMLF.

fMLFKC. The reaction was stirred overnight at room temperature. The excess solvent was removed under reduced pressure. The solid PEGylated product was further reacted with three equivalents of carboxyfluorescein-NHS and 1% DIEA in 500 µl DMF. The reaction was stirred for 3 h at room temperature. The product was then treated with 5 M excess of dithiothreitol (DTT) for another 2 h to remove the thiopyridine protection group on the peptide backbone. The final product was recrystallized from cold ether, washed three times to remove impurities and dried under vacuum. Then the dried product was dissolved in ~5 ml ddH_2O and was dialyzed again ddH_2O for 2 days in the dark. The solution was dried under vacuum to yield the powder of purified product.

Synthesis of Tritium-Labeled PEG-fMLF Nanocarriers

$mPEG_{5K}$-(maleimide)$_2$ (2 mmol) was dissolved in 1 ml phosphate-buffered saline (PBS, pH=7.4) at room temperature. Three equivalents of fMLFKC were added to this. The reaction was stirred overnight at room temperature. The excess solvent was removed under reduced pressure. The solid PEGylated product was further reacted with *N*-succinnimidyl-[2, 3-^{3}H]-propionate and 1% DIEA in 1 ml DMF. The reaction was stirred for 3 h at room temperature and chased by three equivalents of cold propionic anhydride for 3 h. The final product was recrystallized from cold ether, washed three times to remove impurities and dried under vacuum. The control $mPEG_{5K}$-NH_2 and PEG_{20k}-$(NH_2)_4$was directly reacted with *N*-succinnimidyl-[2, 3-^{3}H]-propionate and chased with three equivalents of cold propionic anhydride as described above.

The peptide-backbone nanocarrier acetyl-Cys(thiopyridine)-[β-Ala-β-Ala-Lys(PEG_{5k}-fMLFKC]$_4$-amide was synthesized as described above. The solid PEGylated product was reacted with three equivalents of *N*-succinnimidyl-[2, 3-^{3}H]-propionate and 1% DIEA in 1 ml DMF. The reaction was stirred for 3 hrs at room temperature and chased by cold propionic anhydride for 3 h. The product was further treated with 5 M excess of dithiothreitol (DTT) for another 2 h to remove the thiopyridine protection group on the peptide backbone. The final product was recrystallized from cold ether, washed three times to remove impurities and dried under vacuum.

In Vitro Stability in PBS Buffer and Rabbit Plasma

The stability of the fluorescein-labeled PEG-fMLF nanocarriers was tested in 10 mM PBS (pH 7.4) and rabbit plasma at 37°C for 24 h. The PEG-nanocarriers were incubated separately in 10 mM PBS (pH 7.4) or rabbit plasma at 37°C. Aliquots were withdrawn at different time points and centrifuged at 14,000×*g* for 90 min with a Microcon™ filter (molecular weight cut-off=3,000 Da; Amicon Inc., Beverly, MA). The free fMLF cleaved from the PEG nanocarrier during the incubation passes through the filter whereas the fMLF that remains linked is retained. The eluents and retentates resulting from the different incubation time points were withdrawn and subjected to fluorescence detection. Each measurement was done in triplicate.

The stability of the tritiated PEG-fMLF nanocarriers was tested in 10 mM phosphate buffered saline (pH 7.4) and rabbit plasma at 37°C. One milliliter solutions of $[fMLFK(^3H)C]_2$-$mPEG_{5K}$ and acetyl-C[AAK(PEG_{5K}-fMLFK $[^3H]C$)]$_4$-amide were prepared in PBS (pH 7.4) and plasma to a final concentration of 1 μCi/ml. Aliquots (200 μl) were withdrawn after 24 h incubation. The proteins in plasma were precipitated using 800 μl acetonitrile followed by vortexing for 1 min and centrifuged for 5 min at 6000×*g*. Supernatant (50 μl) was directly injected into the HPLC (HP 1100) equipped with a β-ram radioisotope detector. The column was TSK-GEL G3000PW HPLC column (Tosoh Corp., Japan). The mobile phase was 100% ddH_2O and the flow rate was maintained at 1 ml/min. The decrease in the area of the nanocarrier peak was monitored in triplicate to assess loss due to instability.

Animals

Male Sprague–Dawley rats (jugular vein cannulated, weighing 250–300 g, 2–3 months of age) were purchased from Hilltop Lab Animals, Inc (Scottdale, PA). Female FVB mice, 5 or 6 weeks of age, were purchased from Taconic Farms (Germantown, PA). Animals were maintained on a 12-h light/dark cycle and received laboratory chow and water *ad libitum*. Animals were housed three or four per cage and were allowed to acclimatize to the animal facility for a minimum of 3 days prior to use. These investigations were carried out under established federal regulations and animal protocols approved by the Rutgers University Institutional Animal Care and Use Committee for the care and use of laboratory animals.

Uptake by Mouse Peritoneal Macrophages

Female FVB mice were injected with 5 μl fluorescent PEG-fMLF nanocarriers i.p. and incubated with the peritoneal macrophages for 4 h. Four hours after injection, the mice were killed by cervical dislocation, and each was peritoneally injected with 5 ml of saline. The peritoneum of the mouse was massaged for 1 min and the solution inside the abdominal cavity was withdrawn to recover peritoneal macrophages. Macrophages were washed three times with 1 ml of phosphate buffer. The total cell-associated fluorescence was then analyzed by flow cytometry using a Coulter EPICS PROFILE equipped with a 25 mW argon laser. For each analysis, 10,000 to 20,000 events were accumulated.

Pharmacokinetic and Biodistribution Studies

Male Sprague–Dawley rats (jugular vein cannulated, weighing 250–300 g, 2–3 months of age) were used for PK and biodistribution studies. The animals were dosed intravenously via a tail vein injection with the nanocarriers to be tested (dosing volume: 0.5–1 ml/kg). After dose administration, blood samples (~0.2–0.3 ml/sample) were collected from the catheter at selected time points (0, 1, 5, 10, 15, 30 min and 1, 2, 4, 8 and 24 h) for up to 24 h post dose. After each sample was taken, the catheter was flushed with ~0.3 ml sterile heparinized saline (50 IU/ml) to compensate for blood loss and to prevent the catheter from clotting. Urine and feces were also collected for up to 24 h. At the end of the study, animals were euthanized by intravenous injection of pentobarbital at 100 mg/kg. Selected tissues, such as brain, heart, intestines, liver, lung, spleen, and kidneys were harvested, rinsed with PBS to wash away blood attached around the organs and weighed. Then ~0.1 g tissue specimens were digested in 1 ml of Solvable at 55°C in a water bath for 2 h and cooled to room temperature. Three aliquots of 0.3 ml of 30% hydrogen peroxide were added to samples for decolorization. Scintillation cocktail was added to the decolorized samples, samples were vortexed and the radioactivity of each sample was determined using a liquid scintillation analyzer LSC-3100. Each dose regimen was tested in three rats to achieve adequate statistical power. Plasma concentration–time data are analyzed with two-compartment model methods using WinNonlin (Pharsight Corporation, Mountain View, CA).

Pharmacokinetic Analysis

To determine the disposition of PEG nanocarriers, the plasma concentration–time profile was analyzed using a two-compartment model (WinNonlin v 4.1, Pharsight Corp., Apex, NC, USA). The model can be expressed by Eq. 1:

$$C(T) = A^*\mathrm{EXP}(-\alpha^*T) + B^*\mathrm{EXP}(-\beta^*T) \qquad (1)$$

The pharmacokinetic parameters, A, B, α, and β in Eq. 1 were calculated by WinNonlin. The first-order transfer rate constant from a central compartment (1) to a peripheral compartment (2), k12, the first-order transfer rate constant from a peripheral compartment (2) to a central compartment (1), k21, the elimination constant from the central compartment (1), k10, and the distribution volume of central compartment V1 were calculated by WinNonlin. The half-life at the β-phase of the plasma concentration-time curve was calculated using the parameter β.

Statistical Analysis

All statistical tests were performed using GraphPad Instat (GraphPad Software, Inc., San Diego, CA). A minimal p value of 0.05 was used as the significance level for all tests. One-way analysis of variance and Tukey test was performed on the uptake data. All data are reported as means±SD of three observations, unless otherwise noted. The graphs were plotted using GraphPad Prism 4.01 (GraphPad Software, Inc., San Diego, CA).

RESULTS

Design and Synthesis of PEG-fMLF Nanocarriers

PEG-fMLF nanocarriers $mPEG_{5K}$-fMLF, $mPEG_{5K}$-$(fMLF)_2$, PEG_{10K}-$(fMLF)_4$ were prepared by coupling fMLFKC to $mPEG_{5K}$-maleimide, $mPEG_{5K}$-$(maleimide)_2$ and PEG_{10K}-$(NH_2)_4$ according to the procedures described above (Scheme 1). The novel peptide-backbone nanocarriers were prepared by coupling the peptide backbone, acetyl-Cys(thiopyridine)-(β-Ala-β-Ala-Lys-)$_4$-amide to a heterobifunctional PEG, NHS-PEG-VS. The NHS moiety

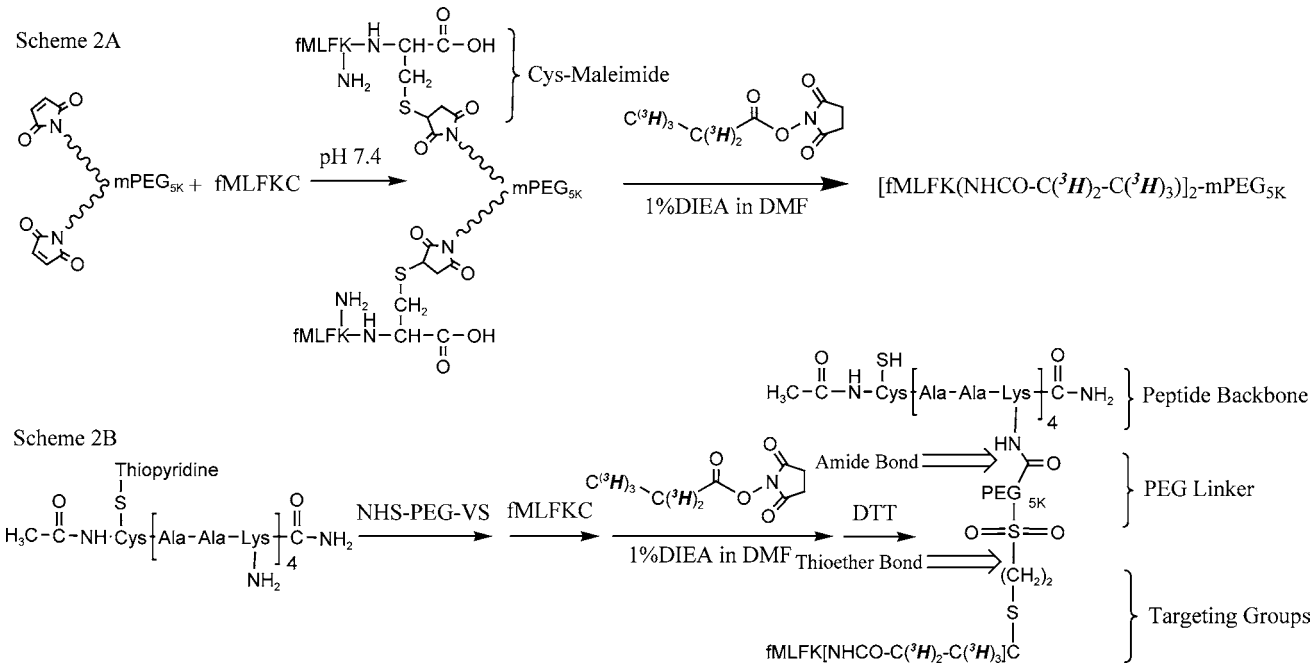

Scheme 2. Synthesis schemes of tritium-labeled PEG-fMLF nanocarriers with 2 (A) and 4 (B) copies of fMLF.

of NHS-PEG-VS reacts specifically with ε-amine groups on lysines of the backbone peptide and the VS group is used for attachment of PEG to the sulfhydryl (SH) moiety of the fMLFKC peptide. The resulting linkages formed are amide (for NHS) or thioether (for VS) bonds between fMLFKC and the peptide backbone. Both bonds are highly stable under physiological conditions. All nanocarriers were purified from low molecular weight contaminants using 3 kDa dialysis bags against ddH_2O for 2 days. The purified products were confirmed by SEC using a TSK G3000PW column and concentrations were determined by amino acid analysis. Amino acid analysis also confirmed the presence of methionine, leucine, phenylalanine, lysine and cysteine at the expected ratio in the final bioconjugate.

The selected PEG-fMLF nanocarriers (Scheme 2) were labeled by tritium by reaction with *N*-succinnimidyl-[2, 3-^{3}H]-propionate and chased with cold propionic anhydride. The final product was recrystallized from cold ether, washed three times to remove impurities and dried under air. The purified products were confirmed by SEC using HP1100 HPLC equipped with a TSK G3000PW column and β-ram radio-detector (Fig. 1).

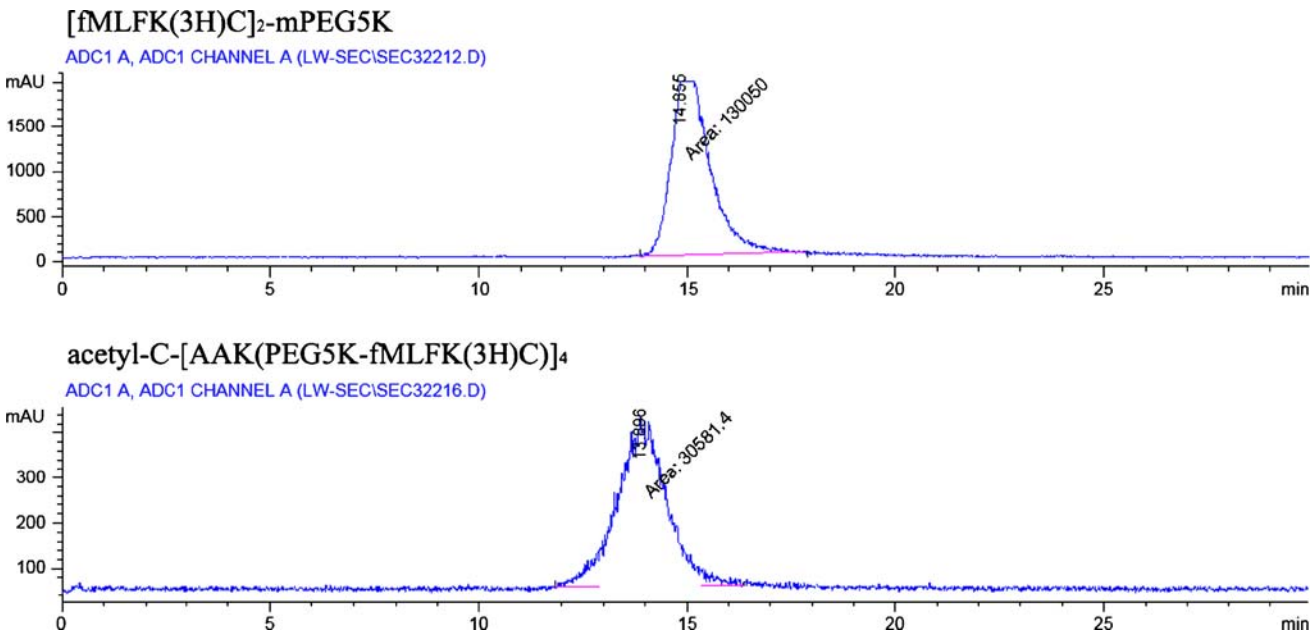

Fig. 1. Size exclusion chromatography of tritium-labeled PEG-fMLF nanocarriers with 2(Scheme 2A) and 4 (Scheme 2B) copies of fMLF. The retention time was 14.9 min for [fMLFK(^{3}H)C]$_2$-mPEG$_{5K}$ and 13.9 min for acetyl-C[AAK(PEG$_{5K}$-fMLFK[^{3}H]C)]$_4$-amide.

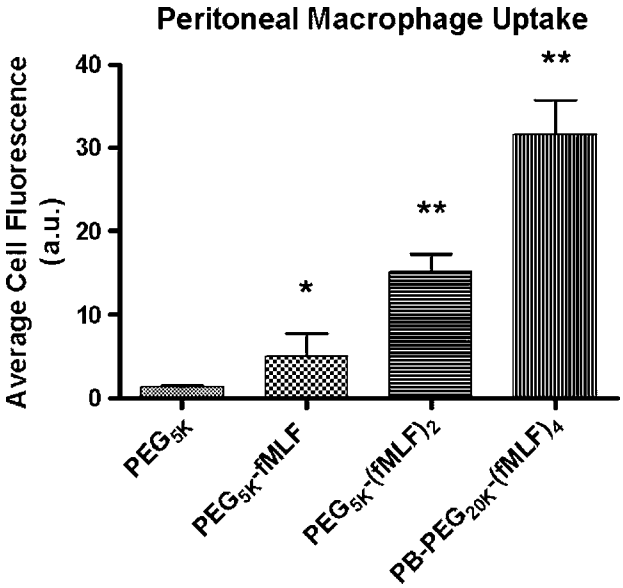

Fig. 2. Uptake of PEG-fMLF nanocarriers in mice peritoneal macrophages at 37°C after 4 h of incubation. Means±SD for three experiments in mice are shown for each value. (*Statistically significant difference between the control PEG_{5K} and PEG-fMLF nanocarriers. $P<0.05$, $^{**}P<0.01$).

Stability of PEG-fMLF Nanocarriers

The stability of the fluorescein-labeled and tritium-labeled PEG-fMLF nanocarriers were tested in 10 mM phosphate buffered saline (pH 7.4) and rabbit plasma at 37°C for 24 h. For $[fMLFK(^3H)C]_2$-$mPEG_{5K}$, thioether bonds linked fMLFKC and $mPEG_{5k}$-(maleimide)2 and an amide linked fMLFKC and tritium-labeled propionate. For acetyl-$C[AAK(PEG_{5k}$-$fMLFK(^3H)C)]_4$ -amide, an amide bond (derived from NHS) or thioether bond (derived from VS) linked fMLFKC to the peptide backbone. As confirmed by simultaneous HPLC and radiolabel detection, all bonds were highly stable under physiological conditions. Both nanocarriers were very stable in PBS and only 3.2% degraded in rabbit plasma during a 24-h incubation.

Uptake by Mouse Peritoneal Macrophages

Injection of PEG-fMLF nanocarriers into the peritoneal cavity of FVB mice was used to determine the *in vivo* macrophage uptake (Fig. 2). The mice in this study were not injected with thioglycolate, and, therefore, the macrophages in the peritoneal cavity were not activated (22). PEG-fMLF enhanced macrophage uptake by 3.8-fold ($p<0.05$) after 4 h of incubation at 37°C compared to the control PEG_{5k}. On the other hand, PEG_{5k}-$(fMLF)_2$ and PEG_{20k}-$(fMLF)_4$ increased uptake by 11.3 and 23.6-fold ($p<0.01$), respectively, compared to the control PEG_{5k}. These results were not surprising since we demonstrated enhanced uptake resulting from the attachment of multiple copies of fMLF in differentiated U937 cells (Bioconj Chem 2007, submitted) and neutrophil-like differentiated HL-60 cells (18). The difference in uptake between nanocarriers with one or two copies of fMLF was less than what was observed *in vitro* but the difference between two and four copies was larger than in cultured cells. These results suggest bioconjugate uptake is enhanced by higher levels of fMLF ligand per PEG nanocarrier in the *in vivo* settings relative to results *in vitro*. However, an effect of PEG size cannot be excluded as explaining this result. The binding to peritoneal macrophages was significantly enhanced with even just one copy of fMLF. This is in direct contrast to the lower binding of such nanocarriers we observed *in vitro* [Bioconj Chem 2007, submitted, (18)].

Pharmacokinetic Studies

The elimination profile of the tritium-labeled control PEG and PEG-fMLF nanocarriers in blood after IV administration is shown in Fig. 3. The experimental data fit well to the theoretical curve, indicating that the injected PEG nanocarriers were eliminated in accordance with a two-compartment model disposition behavior. Table I summarizes the pharmacokinetic parameters of each nanocarrier calculated using a two-compartment model. The elimination profiles and pharmacokinetic analysis reveals a clear difference between nanocarriers with different molecular weights and between nanocarriers with and without fMLF. Both PEG_{5K} and PEG_{5K}-$(fMLF)_2$ were eliminated rapidly from the blood circulation, with half-lives at 14.6 min and 44.9 min, respectively. In the contrast, PEG_{20K} and PEG_{20K}-$(fMLF)_4$ circulated much longer than 5 kDa PEG nanocarriers, with half-lives at 452.9 and 177.1 min, respectively. It should be

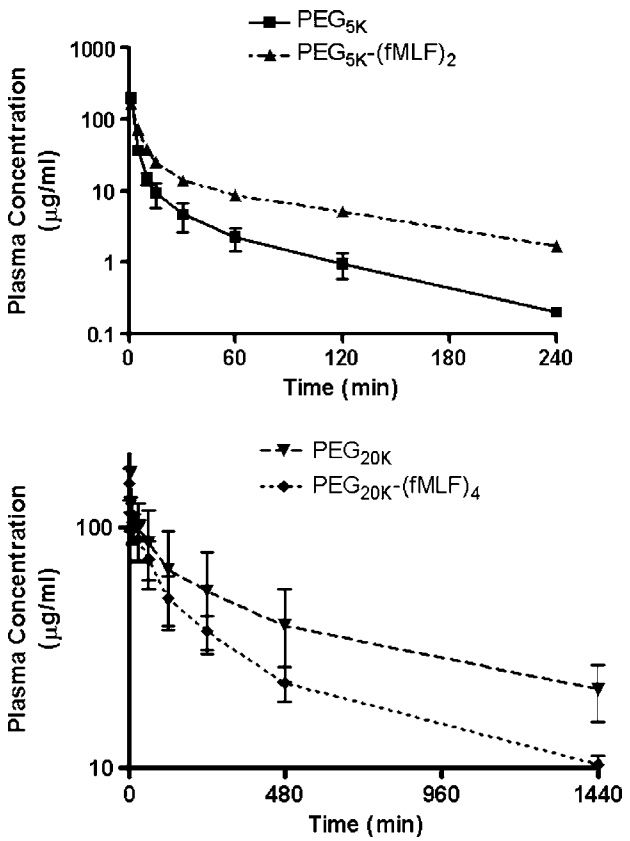

Fig. 3. Plasma clearance of control PEGs and PEG-fMLF nanocarriers carrying two or four fMLF moieties in rats after i.v. injection. Means±SD for rats are shown for each value.

Table I. Pharmacokinetic Parameters of the Control PEGs and PEG-fMLF Nanocarriers Carrying Two or Four fMLF Moieties After i.v. Injection in Rats

Parameter	Units	PEG5K	PEG5K-(fMLF)2	PEG20K	PEG20K-(fMLF)4
AUC	min×μg/ml	1,004.4±186.8	2267.1±308.2	55,220.3±19,890.5	24,493.3±3,194.4
k10_HL	min	2.1±0.1	7.8±2.6	194.0±34.3	107.5±4.0
Alpha	1/min	0.50±0.06	0.27±0.10	0.06±0.01	0.17±0.02
Beta	1/min	0.05±0.01	0.02±0.01	0.0015±0.0002	0.0039±0.0001
Alpha_HL	min	1.3±0.1	2.8±1.0	11.4±1.0	4.0±0.4
Beta_HL	min	14.6±3.0	44.9±22.7	452.9±59.2	177.1±3.5
A	μg/ml	307.2±41.7	182.8±31.1	113.7±22.3	63.2±6.0
B	μg/ml	20.2±3.8	26.8±11.1	80.5±22.6	94.6±13.4
Cmax	μg/ml	327.5±45.5	209.5±42.2	194.2±44.6	157.8±19.0
CL	ml/min	2.64±0.49	0.69±0.09	0.05±0.02	0.11±0.01
AUMC	min×min×μg/ml	10,544.7±5,329.7	106,099.5±62796.8	35,699,901.3±15,901,671.8	6,162,927.3±775158.7
MRT	min	10.181±3.4	45.3±21.5	631.3±86.2	251.7±4.8
Vss	ml	26.1±4.0	30.2±10.6	31.6±7.6	27.1±3.6
V2	ml	18.0±5.1	22.7±9.1	17.8±4.9	10.4±1.7

The pharmacokinetic parameters of the control PEGs and PEG-fMLF nanocarriers were calculated using a two-compartment model by WinNonlin V4.1. Means±SD for three rats are shown for each value.

noted that the attachment of two fMLF peptides to PEG_{5K} increased the half-life about threefold and the area under curve (AUC) about 2.2-fold, respectively, indicating longer plasma residence due to the appended peptides. On the other hand, the attachment of four fMLF peptides to PEG_{20K} decreased the half-life of this longer-persisting PEG by about 60% and AUC by 57%, respectively.

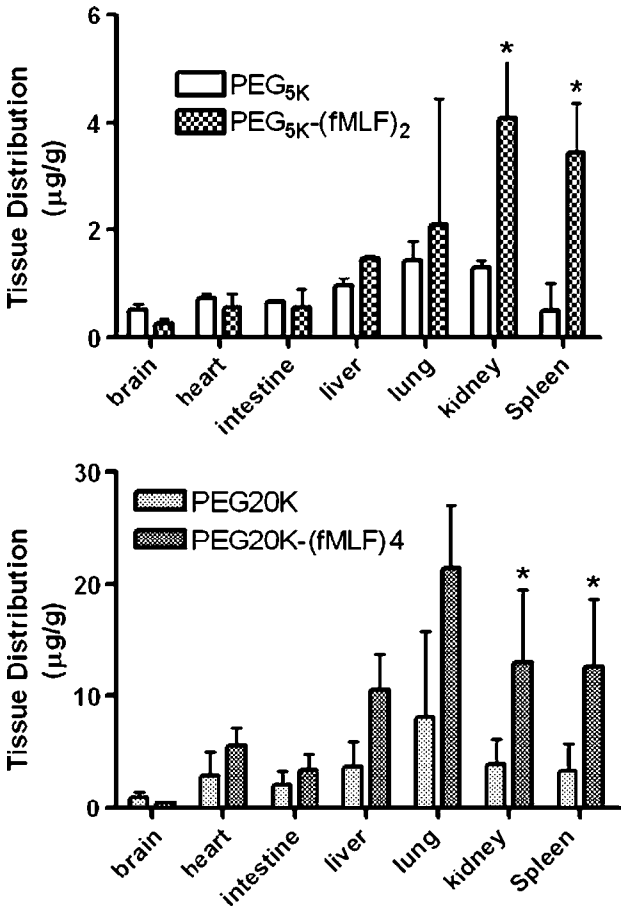

Fig. 4. Tissue distribution of control PEGs and PEG-fMLF nanocarriers carrying two or four fMLF moieties in rats after i.v. injection. Means±SD for three experiments in rats are shown for each value. (*$p<0.05$).

Biodistribution Studies

The tissue distribution of PEG-fMLF nanocarriers are shown as accumulation per gram of tissue in Fig. 4. For PEG molecules without fMLF, radioactivity in the blood was 11% for PEG_{5K} and 42% for PEG_{20K}, consistent with the reduced radioactivity in the urine for the smaller PEG_{5K} (65%) and larger PEG_{20K} (32%; data not shown). The distribution in macrophage-containing tissues revealed significant differences between nanocarriers with and without targeting peptide fMLF. PEG_{5K} accumulated in the lung, kidneys, liver, and to a lesser extend, in the intestine, spleen, heart and brain. The attachment of two copies of fMLF to PEG_{5K} increased the accumulation in major macrophage-containing organs (23) such as kidneys (3.2-fold, $p<0.05$), spleen (6.9-fold, $p<0.05$), lung (1.5-fold) and liver (1.5-fold) but did not significantly affect the accumulation in brain, heart and intestine. The peptide-backbone PEG nanocarrier acetyl-C-$[AAK(PEG)]_4$-amide has molecular weight about 20 kDa and accumulated in the lung, kidneys, liver, and to a lesser extent, in the intestine, spleen, heart and brain. The attachment of four copies of fMLF to acetyl-C-$[AAK(PEG)]_4$-amide increased the accumulation in major macrophage-containing organs such as kidneys (3.3-fold, $p<0.05$), spleen (3.8-fold, $p<0.05$), lung (2.7-fold) and liver (2.8-fold) but did not significantly affect the accumulation in brain, heart and intestine.

DISCUSSION

The clinical potential of anti-HIV agents has been limited by a variety of factors such as drug toxicity in uninfected cells and the development of drug resistance leading to sub-therapeutic drug levels and the formation of viral reservoirs. Better drug delivery and targeting technologies are required to specifically increase target cell exposure to these potent therapeutic agents. Therefore, drug delivery

systems specifically targeted to macrophage cell surface receptors could potentially improve therapeutic efficacy and minimize systemic toxicity of anti-HIV drugs.

Macrophages are considered the first line of defense in the immune response to foreign invaders and have been found to play an important role during HIV-1 infection as both primary targets and major viral reservoirs. Macrophages possess various receptors such as formyl peptide, mannose and Fc receptors, which potentially offer a targeting enhancing option via receptor-mediated endocytosis. A previous report by Pooyan *et al.* (18) illustrated the potential of PEG nanocarrier bearing multiple copies of fMLF for improving *in vitro* macrophage targeting. Recently, we studied the effects of various molecular features of PEG-fMLF nanocarriers such as the number of targeting peptides and PEG sizes on cell uptake in human macrophage-like differentiated U937 cells. The results suggest that appending only two copies of the ligand to the multifunctional nanocarrier was sufficient for optimal binding and the optimal nanocarrier size for improved macrophage uptake *in vitro* was about 20 kDa, which corresponds to a size of about 40 nm.

Effective targeting to macrophages residing in tissues requires that a delicate balance be struck between plasma persistence, tissue distribution, receptor binding and macrophage uptake. Maximizing the circulation half-life of nanocarriers in blood but avoiding a reduction in their penetration into macrophage tissue compartments becomes a significant challenge. By limiting studies to the *in vitro* format, critical *in vivo* processes are ignored that will have a significant impact on drug delivery. Indeed the polymeric portion of the nanocarrier, which often represents the major part of the construct, is more exposed than the drug to the biological environment and has a significant effect on biological targeting and disposition. Thus, our goal was to elucidate the relationship between the *in vivo* dispositional properties and structural characteristics of PEG-fMLF nanocarriers.

PEG was chosen as the pharmaceutical carrier for the macrophage-targeted drug delivery nanocarrier due to its ability to extend elimination half-life, increase stability and decrease immunogenicity of PEGylated pharmaceuticals, especially protein and peptide therapeutics (24–30). It is known that the biopharmaceutical properties of PEG nanocarriers depends strictly on the physicochemical and biological properties of the components of the constructs (which in our study are polymers and targeting moieties), as well as on the properties of the whole nanocarrier (31). The presence of PEG plays an important role in defining the *in vivo* fate of nanocarriers. In the present study, we have shown that increasing molecular weight of PEG-fMLF nanocarriers from 5 to 20 kDa significantly increased the plasma residence. However, studies of PEG in solution showed that each ethylene glycol sub-unit is tightly associated with two or three water molecules. The binding of water to PEG makes PEGylated compounds function as though they are three to nine times larger than a corresponding soluble protein of similar molecular weight (32,33). Clinically used PEG polymers with associated water molecules act like a shield to protect the attached drug from enzymatic degradation, inhibit interactions with cell surface proteins and provide increased size to prevent rapid renal filtration and clearance. These "stealth" properties of PEG have proven to be very valuable in prolonging drug blood levels. However, the reduction of interaction with cell-surfaces due to PEG limits its use as a biomaterial for cell-surface or intracellular drug delivery and targeting. Therefore, the very property of PEGylation that has made it clinically useful and commercially successful also limits its application for drug/nanocarrier targeting to HIV reservoirs or sanctuary sites such as macrophages, the central nervous system and testis. However, the current results showed that by covalent conjugation of macrophage targeting moiety fMLF to PEG, it is possible to achieve a higher accumulation in macrophages residing in tissues.

A 20 kDa peptide-backbone PEG nanocarrier acetyl-Cys-[β-Ala-β-Ala-Lys(PEG_{5k}-fMLFKC]$_4$-amide with branched shape and multiple coupling sites was shown to be the optimal structure tested for facilitating the delivery of PEG-fMLF nanocarriers to the macrophage-residing tissues and its ability to circulate for a long period of time in the blood. A branched PEG 'acts' as if it were much larger than a corresponding linear PEG of the same molecular mass. A linear PEG is distributed throughout the body with a larger distribution while a branched PEG is distributed with a smaller distribution and early on delivered to the liver and spleen (34). The increase in the hydrodynamic size of $F(ab)_2$ form of a humanized anti-interleukin-8 (anti-IL-8) antibody was about sevenfold by adding one 20 kDa PEG and about 11-fold by adding one branched 40 kDa (35). The F(ab′)2 conjugate obtained by linking a single branched 40 kDa PEG was found to possess an apparent size of 1,600 kDa (protein equivalent), greatly over the kidney ultrafiltration limit, and an AUC after intravenous administration 15.7 higher than the unmodified protein (35). Branched PEGs are also better at cloaking attached drugs thereby reducing antigenicity and the likelihood of destruction (36). The binding of branched 10 kDa PEG to asparaginase reduced the antigenic character of the protein about tenfold as compared to the counterpart obtained by modification with 5 kDa PEG (37). These results are attributable to the higher molecular weight and "umbrella like" structure of the branched polymer, which efficiently prevents the approach of anti-protein antibodies and immunocompetent cells.

Macrophages possess various receptors such as formyl peptide receptors, mannose receptors, Fc receptors, complement and many other receptors (19–21). These surface receptors determine the control of activities such as activation, recognition, endocytosis, secretion etc. A number of natural ligands for macrophage targeting have been explored. It was shown by Muller and Schuber that mannose residue-conjugated liposomes were associated to peritoneal macrophages and Kupffer cells in about two to four times greater amount than were plain unconjugated liposomes (38). The acetylated low density lipoprotein (AcLDL), a ligand for macrophage scavenger receptors, was conjugated to AZT and showed tenfold more uptake than AZT alone by a murine macrophage cell line J774.A and a human macrophage cell line U937 (39). In the present study, the peptide fMLF was chosen as the targeting moiety for formyl peptide receptor on macrophages because: (1) formyl peptide receptors are specifically expressed on phagocytic cells such as macrophages, dendritic cells and neutrophils; (2) fMLF specifically binds to formyl peptide receptors on macrophages with high affinity; (3) down-regulation of CCR5 co-

receptor by fMLF could potentially inhibit the viral entry into macrophages, which could result in additional therapeutic effects for anti-HIV drugs targeted to FPR. The attachment of two or four fMLF residues significantly increased uptake in peritoneal macrophages. The pharmacokinetic properties and tissue distribution revealed further differences between nanocarriers with and without targeting peptide fMLF. However, the impact was different among PEG nanocarriers with different molecular weights. The threefold increase of the half-life $t_{1/2}$ by attachment of two fMLF peptides to PEG_{5K} could be because two fMLF residues increased the molecular weight of the nanocarrier by about 1,450 Da. The possibility of enhanced interactions of PEG_{5K}-$(fMLF)_2$ with monocytes, neutrophils or other cells in blood, which might also increase plasma residence time and decrease the renal clearance, cannot be ruled out. On the other hand, the 40% decrease of the half-life $t_{1/2}$ by attachment of four fMLF peptides to PEG_{20K} is consistent with the observed enhanced accumulation in macrophage-rich tissues such as liver, kidneys and spleen, which indicated a non-renal mechanism of clearance from the circulation. The results demonstrated that the attachment of macrophage targeting moiety (fMLF) to 5 kDa and 20 kDa PEG increases accumulation of PEG nanocarriers in target macrophage-rich tissues. This targeting ability, combined with the prolonged plasma residence of 20 kDa PEG, makes the acetyl-C-$[AAK(PEG_{5K}\text{-fMLF})]_4$-amide the most promising nanocarrier tested for improving macrophage targeting *in vivo*. In conclusion, we characterized the *in vivo* peritoneal uptake, pharmacokinetics and biodistribution of PEG-fMLF nanocarriers. The results demonstrate increased accumulation of the PEG nanocarriers with multiple copies of fMLF in peritoneal macrophages and macrophages residing in other tissues (e.g. liver, kidneys and spleen). This targeting ability, combined with the prolonged plasma residence of 20 kDa PEG, makes the acetyl-C-$[AAK(PEG_{5K}\text{-fMLF})]_4$-amide the most promising nanocarrier tested to date for improving macrophage targeting *in vivo*.

ACKNOWLEDGEMENTS

This work was supported by grants AI 33789 and AI 51214 from National Institutes of Health.

REFERENCES

1. A. M. Vandamme, K. Van Vaerenbergh, and E. De Clercq. Anti-human immunodeficiency virus drug combination strategies. *Antivir. Chem. Chemother.* **9**:187–203 (1998).
2. D. R. Bangsberg, F. M. Hecht, E. D. Charlebois, A. R. Zolopa, M. Holodniy, L. Sheiner, J. D. Bamberger, M. A. Chesney, and A. Moss. Adherence to protease inhibitors, HIV-1 viral load, and development of drug resistance in an indigent population. *AIDS* **14**:357–366 (2000).
3. L. K. Schrager and M. P. D'Souza. Cellular and anatomical reservoirs of HIV-1 in patients receiving potent antiretroviral combination therapy. *JAMA* **280**:67–71 (1998).
4. D. D. Richman. HIV chemotherapy. *Nature* **410**:995–1001 (2001).
5. R. Langer. Drug delivery and targeting. *Nature* **392**:5–10 (1998).
6. R. Langer. Drug delivery. Drugs on target. *Science* **293**:58–59 (2001).
7. V. P. Torchilin. Drug targeting. *Eur. J. Pharm. Sci.* **11**(Suppl 2): S81–S91 (2000).
8. H. Schuitemaker, N. A. Kootstra, R. E. de Goede, F. de Wolf, F. Miedema, and M. Tersmette. Monocytotropic human immunodeficiency virus type 1 (HIV-1) variants detectable in all stages of HIV-1 infection lack T-cell line tropism and syncytium-inducing ability in primary T-cell culture. *J. Virol.* **65**:356–363 (1991).
9. S. Aquaro, R. Calio, J. Balzarini, M. C. Bellocchi, E. Garaci, and C. F. Perno. Macrophages and HIV infection: therapeutical approaches toward this strategic virus reservoir. *Antiviral Res.* **55**:209 (2002).
10. F. Ahsan, I. P. Rivas, M. A. Khan, and A. I. Torres Suarez. Targeting to macrophages: role of physicochemical properties of particulate carriers—liposomes and microspheres—on the phagocytosis by macrophages. *J. Control Release*. **79**:29–40 (2002).
11. T. Igarashi, C. R. Brown, Y. Endo, A. Buckler-White, R. Plishka, N. Bischofberger, V. Hirsch, and M. A. Martin. Macrophage are the principal reservoir and sustain high virus loads in rhesus macaques after the depletion of CD4+ T cells by a highly pathogenic simian immunodeficiency virus/HIV type 1 chimera (SHIV): Implications for HIV-1 infections of humans. *Proc. Natl. Acad. Sci. U S A* **98**:658 (2001).
12. D. Marras, L. A. Bruggeman, F. Gao, N. Tanji, M. M. Mansukhani, A. Cara, M. D. Ross, G. L. Gusella, G. Benson, V. D. D'Agati, B. H. Hahn, M. E. Klotman, and P. E. Klotman. Replication and compartmentalization of HIV-1 in kidney epithelium of patients with HIV-associated nephropathy. *Nat. Med.* **8**:522–526 (2002).
13. R. W. Price, B. Brew, J. Sidtis, M. Rosenblum, A. C. Scheck, and P. Cleary. The brain in AIDS: central nervous system HIV-1 infection and AIDS dementia complex. *Science* **239**:586–592 (1988).
14. D. D. Ho, T. R. Rota, R. T. Schooley, J. C. Kaplan, J. D. Allan, J. E. Groopman, L. Resnick, D. Felsenstein, C. A. Andrews, and M. S. Hirsch. Isolation of HTLV-III from cerebrospinal fluid and neural tissues of patients with neurologic syndromes related to the acquired immunodeficiency syndrome. *N. Engl. J. Med.* **313**:1493–1497 (1985).
15. J. Stebbing, B. Gazzard, and D. C. Douek. Where does HIV live? *N. Engl. J. Med.* **350**:1872–1880 (2004).
16. S. M. Crowe and S. Sonza. HIV-1 can be recovered from a variety of cells including peripheral blood monocytes of patients receiving highly active antiretroviral therapy: a further obstacle to eradication. *J. Leukoc. Biol.* **68**:345–350 (2000).
17. S. Sonza, H. P. Mutimer, R. Oelrichs, D. Jardine, K. Harvey, A. Dunne, D. F. Purcell, C. Birch, and S. M. Crowe. Monocytes harbour replication-competent, non-latent HIV-1 in patients on highly active antiretroviral therapy. *AIDS* **15**:17–22 (2001).
18. S. Pooyan, B. Qiu, M. M. Chan, D. Fong, P. J. Sinko, M. J. Leibowitz, and S. Stein. Conjugates bearing multiple formyl-methionyl peptides display enhanced binding to but not activation of phagocytic cells. *Bioconjug. Chem.* **13**:216–223 (2002).
19. E. R. Prossnitz and R. D. Ye. The N-formyl peptide receptor: a model for the study of chemoattractant receptor structure and function. *Pharmacol. Ther.* **74**:73–102 (1997).
20. B. Burke and C. E. Lewis. The macrophage. Oxford University Press, Oxford, New York, 2002.
21. B. Vernon-Roberts. The macrophage. University Press, Cambridge [Eng.], 1972.
22. P. C. Leijh, T. L. van Zwet, M. N. ter Kuile, and R. van Furth. Effect of thioglycolate on phagocytic and microbicidal activities of peritoneal macrophages. *Infect. Immun.* **46**:448–452 (1984).
23. S. Maesaki. Drug delivery system of anti-fungal and parasitic agents. *Curr. Pharm. Des.* **8**:433–440 (2002).
24. A. Kozlowski and J. M. Harris. Improvements in protein PEGylation: pegylated interferons for treatment of hepatitis C. *J. Control. Release* **72**:217–224 (2001).
25. J. M. Harris, N. E. Martin, and M. Modi. Pegylation: a novel process for modifying pharmacokinetics. *Clin. Pharmacokinet.* **40**:539–551 (2001).
26. A. Kozlowski, S. A. Charles, and J. M. Harris. Development of pegylated interferons for the treatment of chronic hepatitis C. *BioDrugs* **15**:419–429 (2001).

27. C. D. Conover, R. B. Greenwald, A. Pendri, C. W. Gilbert, and K. L. Shum. Camptothecin delivery systems: enhanced efficacy and tumor accumulation of camptothecin following its conjugation to polyethylene glycol via a glycine linker. *Cancer Chemother. Pharmacol.* **42**:407–414 (1998).
28. R. B. Greenwald. PEG drugs: an overview. *J. Control. Release* **74**:159–171 (2001).
29. R. B. Greenwald, Y. H. Choe, J. McGuire, and C. D. Conover. Effective drug delivery by PEGylated drug conjugates. *Adv. Drug Deliv. Rev.* **55**:217–250 (2003).
30. M. J. Roberts, M. D. Bentley, and J. M. Harris. Chemistry for peptide and protein PEGylation. *Adv. Drug Deliv. Rev.* **54**:459–476 (2002).
31. P. Caliceti and F. M. Veronese. Pharmacokinetic and biodistribution properties of poly(ethylene glycol)-protein conjugates. *Adv. Drug Deliv. Rev*. **55**:1261–1277 (2003).
32. J. M. Harris. *Poly(ethylene glycol) chemistry: biotechnical and biomedical applications*. Plenum, New York, 1991.
33. M. R. Sherman, L. D. Williams, M. C. P. Saifer, J. A. French, L. W. Kwak, and J. J. Oppenheim. Conjugation of high, molecular weight poly(ethylene glycol) to cytokines: granulocyte-macrophage colony stimulating factors as model substrates. ACS, Washington, DC, 1997.
34. P. Caliceti, O. Schiavon, and F. M. Veronese. Biopharmaceutical properties of uricase conjugated to neutral and amphiphilic polymers. *Bioconjug. Chem.* **10**:638–646 (1999).
35. I. L. Koumenis, Z. Shahrokh, S. Leong, V. Hsei, L. Deforge, and G. Zapata. Modulating pharmacokinetics of an anti-interleukin-8 F(ab′)(2) by amine-specific PEGylation with preserved bioactivity. *Int. J. Pharm.* **198**:83–95 (2000).
36. F. M. Veronese, P. Caliceti, and O. Schiavon. Branched and linear poly(ethylene glycol): Influence of the polymer structure on enzymological, pharmacokinetic, and immunological properties of protein conjugates. *J. Bioact. Compat. Polym.* **12**:196–207 (1997).
37. C. Monfardini, O. Schiavon, P. Caliceti, M. Morpurgo, J. M. Harris, and F. M. Veronese. A branched monomethoxypoly (ethylene glycol) for protein modification. *Bioconjug. Chem.* **6**:62–69 (1995).
38. S. Crowe, T. Zhu, and W. A. Muller. The contribution of monocyte infection and trafficking to viral persistence, and maintenance of the viral reservoir in HIV infection. *J. Leukoc. Biol.* **74**:635 (2003).
39. J. Hu, H. Liu, and L. Wang. Enhanced delivery of AZT to macrophages via acetylated LDL. *J. Control. Release* **69**:327–335 (2000).